HHS Public Access

Author manuscript

Magn Reson Med. Author manuscript; available in PMC 2023 July 01.

Published in final edited form as:

Magn Reson Med. 2022 July ; 88(1): 28–37. doi:10.1002/mrm.29196.

Interleaved Fluid-attenuated Inversion Recovery (FLAIR) MRI and Deuterium Metabolic Imaging (DMI) on human brain in vivo

Yanning Liu[2], **Henk M. De Feyter**[1], **Robert K. Fulbright**[1], **Scott McIntyre**[1], **Terence W. Nixon**[1], **Robin A. de Graaf**[1,2]

[1]Magnetic Resonance Research Center (MRRC), Department of Radiology and Biomedical Imaging

[2]Biomedical Engineering, Yale University, New Haven, CT, United States

Abstract

Purpose: To integrate Deuterium Metabolic Imaging (DMI) with clinical MRI through an interleaved MRI and DMI acquisition workflow. Interleaved MRI-DMI was enabled with hardware and pulse sequence modifications, and the performance was demonstrated using Fluid-attenuated inversion recovery (FLAIR) MRI as an example.

Methods: Interleaved FLAIR-DMI was developed by interleaving the ^{2}H excitation and acquisition time windows into the intrinsic delay periods presented in the FLAIR method. All ^{2}H MR signals were up-converted to the ^{1}H Larmor frequency using a custom-built hardware unit, which also achieved frequency and phase locking of the output signal in real-time. The interleaved measurements were compared with direct measurements both in phantom and in the human brain in vivo.

Results: The interleaved MRI-DMI acquisition strategy allowed simultaneous detection of FLAIR MRI and DMI in the same scan time as a FLAIR-only MRI acquisition. Both phantom and in vivo data showed that the MR image quality, DMI sensitivity as well as information content were preserved using interleaved MRI-DMI.

Conclusion: The interleaved MRI-DMI technology can be used to extend clinical MRI protocols with DMI, thereby offering a metabolic component to the MR imaging contrasts without a penalty on patient comfort or scan time.

Keywords

deuterium metabolic imaging (DMI); fluid-attenuated inversion recovery (FLAIR); interleaved acquisition; human brain

Introduction

Magnetic resonance imaging and spectroscopy are powerful tools in evaluating tissue anatomy and physiology in vivo. Clinically, the majority of the MR applications are focused

Corresponding author: Robin A. de Graaf, The Anlyan Center (TAC), N145, 300 Cedar Street, New Haven, CT 06520-8043, Tel: 203-785-6203, Fax: 203-785-6643, robin.degraaf@yale.edu.

on MRI, where water proton properties are used to examine anatomical information and identify tissue characteristics.[1–3] Apart from structural changes captured by MRI, aberrant metabolism is also an essential character of neurological disorders including but not limited to brain tumors[4,5], neurodegenerative diseases[6] and acute stroke[7]. Supplementing MRI with metabolic information can therefore widen the diagnostic horizon in detecting, characterizing and treating various diseases.

Deuterium metabolic imaging (DMI) is an emerging method to obtain metabolic information in vivo.[8] It combines 3D phase-encoded deuterium magnetic resonance spectroscopic imaging and non-radioactive ^{2}H-labeled substrates (i.e. ^{2}H labeled glucose) administration to spatially map active metabolism. Since its development, DMI has been used to evaluate glucose metabolism in healthy animal[9] and human[8] brain, to characterize glioblastoma brain tumors (GBM) in humans[8] and animals[10] via the Warburg effect, and to assess brown adipose tissue[11] as well as myocardial tissue[12]. Most recently, the performance of DMI has been demonstrated at 9.4T[13], substantiating the previous sensitivity prediction[14]. In addition to its promising performance and extensive applications, DMI is robust and simple to perform, suggesting a high potential to be transformed into a clinical metabolic imaging method.

Despite the benefits of supplementing clinical MRI with DMI, the sequential acquisition of standard MRI and DMI may be too time-consuming and compromise patient compliance. Interleaved acquisition of MRI and an X-nucleus-based MR method is an excellent strategy to reduce scan time without sacrificing data quality.[15–23] The principle of interleaved MR acquisitions has been demonstrated over four decades ago in the field of multi-nuclear NMR.[17,18] In particular, it refers to the sequential acquisition of Larmor frequencies from different nuclei in a time span shorter than the repetition time of the sequence. In an interleaved measurement, the acquisition windows, and possibly also the RF and gradient pulses, are set up independently without mutual overlap. It provides a high level of sequence design flexibility and allows implementation on MR scanners with minimal hardware modification. For these reasons, interleaved acquisition is used to extend MRI with DMI in the MR method described here. Simultaneous acquisition[17,21] is another frequently used approach to achieve accelerated multi-nucleus measurements. A common example of simultaneous ^{1}H-^{2}H MR can be found in high resolution NMR by default where the ^{2}H channel is used to track and lock frequency changes. In contrast to the interleaved methods, independent transmit/receiver for the second nucleus is required and the effect of gradients is often shared among the different nuclei during a simultaneous acquisition. Thus, simultaneous acquisitions have higher technical demands, lower sequence design flexibility and was therefore not chosen for combining MRI and MRS-based acquisitions.

Interleaved multi-nuclear NMR implementations for human clinical research have not been reported until recently[19–21,24], possibly due to the lack of clinically viable non-proton-based metabolic imaging. The potential and robustness of DMI makes it an ideal candidate for interleaved MRI-DMI acquisitions. One hurdle for interleaved multi-nuclei measurements is that most modern (clinical) MRI scanners are optimized to receive signal at only a single Larmor frequency (i.e. ^{1}H) within a given RF pulse sequence, thus requiring additional hardware to achieve successive dual-nucleus acquisition.[19,21,22]

Here we present our solution to interleaved dual-nucleus acquisition - a customized frequency-conversion unit that upconverts the ^{2}H signal to the ^{1}H signal receive path and achieves frequency and phase locking on ^{2}H data in real-time. Using fluid-attenuated Inversion recovery (FLAIR) MRI as an example for a clinical MRI scan, we demonstrate the interleaved acquisition of FLAIR and DMI in the same scan time as a FLAIR-only MRI scan. The performance of FLAIR-DMI in both phantom and human brain in vivo is compared with direct (non-interleaved) acquisitions.

Methods

MR System

Studies were performed on a 4T Magnex magnet (Magnex Scientific Ltd.) interfaced to a Bruker Avance III HD spectrometer controlled via ParaVision 6 (Bruker, Billerica, MA). The system was equipped with actively shielded gradients capable of switching 30 mT/m in 1150 μs and provided up to second-order shimming. The phantom and the in vivo measurements were conducted using a custom-built ^{1}H-^{2}H probe (Fig. 1A), with a 28.5-cm-diameter transverse electromagnetic (TEM) volume coil tuned to ^{1}H (170.5 MHz) and a four-coil Tx/Rx phased array tuned to ^{2}H (26.2 MHz).

Phase and Frequency Locking Up-conversion Unit

For MR systems without intrinsic multi-frequency receive capabilities, the implementation of interleaved signal acquisition can be achieved by adapting all ^{1}H and non-^{1}H frequencies to a single, common frequency, before sending the signal to the systems' receive path. On our Bruker 4 T system, interleaved ^{1}H/^{2}H signal acquisition was achieved by upconverting all ^{2}H signals to the ^{1}H frequency via a custom-built frequency-conversion unit (Fig. 1B, C). The unit consists of an RF mixer, an RF switch and a Direct Digital Synthesizer (DDS) Local Oscillator (LO). As shown in the schematic drawing (Fig. 1B), the ^{1}H signal is sent to one arm of an RF switch. The ^{2}H (26.2 MHz) signal is supplied to an RF mixer and up-converted to ^{1}H (170.5 MHz) by mixing with the 144.3 MHz Direct Digital Synthesizer (DDS) Local Oscillator (LO). The transformed signal is then band-pass filtered, amplified and sent to the other arm of the RF switch. To minimize channel-to-channel and external noise interference, the individual ^{2}H channels are shielded by brass walls (Fig. 1C). During the acquisition, the switching for the correct RF path is defined by TTL trigger pulses in the scanners pulse program (PPG). The LO signal is gated and only present for the ^{2}H portion of the acquisition to prevent interference during the ^{1}H experiment. The use of independent frequency sources for the Bruker ^{2}H signal and the intermediate LO, leads to a reproducible phase roll of the upconverted ^{2}H signal that is dependent on the sequence timings. An effective phase (and frequency) lock of the upconverted ^{2}H signal is achieved by controlling the phase (and frequency) of the LO through a field-programmable gate array (FPGA) via TTL triggers embedded in the pulse sequence. For the final FLAIR-DMI sequence configuration, phase (and frequency) variations are measured on a phantom, stored as an array and played out in synchrony with the pulse sequence to counteract phase and frequency progressions of interleaved ^{2}H signal in real time. No phase/frequency corrections were applied post-acquisition.

Interleaved MRI-DMI Sequence

FLAIR MRI is interleaved with DMI by utilizing the delays inherent to the MRI sequence, while maintaining a constant DMI TR of 314 ms (Fig. 2). Multi-slice (14 slices of 3 mm) FLAIR ($TR/TI/TE_{eff}$ = 8800/2200/90 ms, 2 averages) MRIs were collected as a 256 × 192 matrix over 256 × 192 mm^2 field of view (FOV). The fast spin-echo sequence element intrinsic to FLAIR was executed with eight echoes per excitation (inter-echo spacing 22.5 ms) and 5.7/3.3 ms Gaussian RF pulses for excitation and (partial 135°) refocusing. With an acquisition time of 80 ms and a TR of 314 ms, a total of 28 DMI acquisitions could be interleaved during each MRI repetition. DMI was acquired as a 13 × 9 × 11 matrix over 260 × 180 × 220 mm^3 using a 0.5 ms non-selective square excitation pulse (FA=90°). Using spherical encoding, a complete DMI dataset consisted of 491 phase encoding steps. For a total FLAIR acquisition time of 7 minutes, two complete averages of DMI (NA=2) were acquired without prolonging the experimental duration. While the MRI and DMI acquisition matrices can be chosen as desired, the Bruker Paravision 6.0 environment mandated identical acquisition bandwidths for MRI and DMI. All data was acquired over a 50 kHz spectral width, after which the DMI data was down-sampled to 5 kHz using a lowpass IIR filter (Chebyshev Type I, order 8) post-acquisition.

Phase Correction Measurements

Phase progression of the interleaved ^2H signal was determined on an external D_2O phantom by removing the phase encodings of the DMI acquisitions. The frequency of the external D_2O phantom could be separated from in vivo brain water through a magnetic-susceptibility-induced frequency shift. Specifically, a 1 mL spherical, glass sphere of D_2O (ID 0.6 cm) was placed between two 20 mm diameter niobium plates, causing a homogeneous magnetic field shift of circa 5 ppm. The measured phase was subsequently used to control the LO such that the upconverted ^2H signal remains phase locked. The phase correction list was tested 0, 1, 7 and 30 days after it was generated to ensure phase stability of the interleaved ^2H signal over time.

Phantom measurements

A phantom containing ~ 0.5 % D_2O and various amounts of DMSO-D_6 (0 – 0.05%) was used for all in vitro studies. Interleaved measurements were acquired using the interleaved FLAIR-DMI sequence. Direct (single nucleus acquisitions with standard Bruker hardware) DMI (TR = 314 ms) with an identical phase encoding scheme was obtained subsequently for quantitative comparison with the interleaved acquisition.

In vivo measurements

All human studies were approved by Yale University Institutional Review Board. Natural abundance (N = 2), and [6,6'−$^2H_2$]-glucose enriched DMI (N = 2) were obtained on healthy volunteers. In the [6,6'−$^2H_2$]-glucose enriched measurements, data were acquired 60–75 min after oral intake of 55 g of [6,6'−$^2H_2$]-glucose dissolved in 250 mL of water, as described previously[8]. The global ^2H NMR spectra (TR = 314 ms, NA = 100) and DMI were measured using direct acquisition scheme followed by the identical acquisitions using interleaved FLAIR-DMI scheme.

Data processing

^{1}H MRI and ^{2}H DMI data were processed individually in Matlab R2020b (The Mathworks, Natick, MA, USA). Following k-space reshuffling, the FLAIR MRIs were reconstructed via 2D fast Fourier transformation (FFT). The ^{2}H signals were down-sampled to 5 kHz using the Matlab "decimate" function, extrapolated to the timepoint right after excitation using sigular value decomposition (SVD), fitted and processed using an in-house developed graphical user interface DMIWizard[25]. 5 Hz exponential apodization was applied to the phantom data to reduce spectral artifacts related to FID truncation of the long-lasting in vitro signals. The spectral fitting was based on a linear combination of model spectra (LCM) through least-squares minimization, using Lorentian line shape and zero-order baseline estimation. The signal-to-noise ratio (SNR) was defined as $\mathrm{SNR} = \frac{\mathrm{Area(peak\ of\ interest)}}{\mathrm{SD(Noise)}}$, where the area under the peak is obtained by numerical integration on in vitro data or extracted from the spectral fit for in vivo data. The standard deviation (SD) of the noise was obtained from the empty spectral region between −113 and −102 ppm following linear baseline correction.

Results

Upon frequency-conversion, a phase accumulation was produced in the interleaved ^{2}H signal due to the frequency difference between the system receivers' LO and that of the mixer LO[23].(Fig. 3) The phase accumulation appeared to be predominantly linear, with small deviations as a result of imperfect sequence timing.(Fig. 3A) The phase progression of a sequence was observed to be reproducible so long as the sequence timing remains unchanged. Consequently, a phase list was measured on a D_2O phantom and used to perform phase locking such that the interleaved acquisitions remain in an identical phase throughout the measurements.(Fig. 3D) The phase stability of phase locked ^{2}H signals was measured over the course of 30 days using a predetermined phase list. Fig. 3B shows the phase standard deviation (SD) of the ^{2}H signal as determined over the total duration of a FLAIR MRI scan (2 repetitions spanning 7 minutes of acquisition). The SD of phase locked signal is comparable to that of the direct signal proving the effectiveness of the list approach to correct the phase progression. Moreover, the signal remained phase locked over time, with a merely 0.13 degree increase in SD in one month, confirming that a single, predetermined phase list can be reused for the period of time tested.

The FLAIR MRI and DMI acquired on a phantom containing D_2O and DMSO-D_6 using **(A)** interleaved FLAIR-DMI and **(B)** direct DMI (single nucleus, direct acquisitions) are shown in Fig. 4. High quality ^{2}H localized spectra were observed in both interleaved **(D)** and direct **(E)** measurements. The linewidth and SNR in the localized spectra on the displayed axial section were then compared (Fig. 4C, F), voxel by voxel, to show that there are no significant linewidth and SNR differences between the direct and interleaved DMI datasets. Consequently, the information content and spectral resolution between the direct and interleaved DMI data are equivalent, underlining that MRI and DMI can be acquired in parallel without reducing data quality. Since the ^{1}H channel is a direct feedthrough (Fig. 1B), no differences were expected nor observed for interleaved versus direct MRI.

Fig. 5A shows unlocalized, global ^{2}H MR spectra acquired from human brain in vivo circa 60 min following the oral administration of [6,6'–$^{2}H_2$]-glucose. The close visual correspondence between direct and interleaved ^{2}H MR data was confirmed with a quantitative comparison on linewidth and SNR (Fig. 5B, C).

Fig. 6A shows interleaved FLAIR-DMI obtained from human brain in vivo following the oral administration of deuterated glucose. The DMI data represents one axial (13 × 9) plane extracted from a 3D (13 × 9 × 11) DMI dataset, whereas the FLAIR MRI represents one axial slice from a 14-slice dataset. The DMI data displays the familiar spectral fingerprint of water, glucose and glutamate+glutamine as reported previously[8]. Additional FLAIR MRIs extracted from the same 14-slice dataset (Fig. 6C) show the characteristic minimal image contrast between grey and white matter, and elimination of ventricular water signal.

Discussion

We have successfully demonstrated the interleaved acquisition of FLAIR MRI with DMI, using the same scan time as that of an equivalent FLAIR-only MRI scan, without any degradation in MRI or DMI sensitivity, data quality or information content. The interleaved acquisition strategy provides a practical solution to supplement ^{1}H-based MRI with non-^{1}H-based metabolic imaging without compromising patient comfort or compliance, while maintaining the original MRI contrast and acquisition parameters. It has the potential to become the standard mode of operation for DMI studies in a clinical environment

Our interleaving methodology exploits the inherent delays in the proton MRI pulse sequence to incorporate ^{2}H pulse acquisitions. The relatively short ^{2}H T_1 (70 – 350 ms) suggests that ^{2}H signal can be acquired using a shorter TR, allowing the insertion of multiple ^{2}H pulse acquisitions in one MRI TR, thereby maximizing the time efficiency and/or sensitivity. DMI is especially suitable for interleaved imaging thanks to its simple excitation-acquisition scheme and minimal RF power required. It is also less sensitive to global field inhomogeneity, allowing high quality spectroscopic data acquisition with standard second-order B_0 shimming.

We selected FLAIR as an example to demonstrate the interleaved MRI-DMI methodology because it is a widely used clinical method to detect lesion.[26–29] Furthermore, the FLAIR sequence consists of extensive waiting periods during which ^{2}H windows can be incorporated. Most of the previously reported interleaved multi-nuclear acquisitions have relatively simple interleaving strategies, with one secondary nucleus window interleaved into the inter-excitation delays of the primary nucleus sequence.[17,21,23,24] The interleaved FLAIR-DMI sequence we developed employs a more complex scheme, in which ^{2}H pulse-acquisition windows are inserted after both the inversion pulse and ^{1}H acquisition window. The ^{1}H signal is exempt from the influence of ^{2}H gradients during inversion time as it remains along the z direction.

The same interleaving strategy can, in principle, be extended to other MRI methods that satisfies the following conditions. First, the ^{2}H pulse-acquisition window should be placed such that the gradients for ^{2}H signal do not affect the ^{1}H signal and vice versa. Second,

a sufficiently long ^{2}H acquisition window (circa 80 ms) is allowed, to ensure a complete record of ^{2}H signal. Third, ^{2}H pulses can be integrated equidistantly such that the steady-state of ^{2}H signal is maintained. Alternatively, equilibrium dummy pulses can be used to re-establish the steady state condition. In the interleaved FLAIR-DMI sequence, the ^{2}H TR (=314 ms) was chosen based upon the FLAIR sequence timing, however, a range of ^{2}H TRs can be selected to meet the desired DMI temporal resolution and specific MRI sequence timing requirements. By expanding the interleaved sequence to other clinical relevant MRI scans (i.e. T_1, T_2, diffusion and susceptibility-weighted MRI), a complete interleaved MRI-DMI brain imaging protocol can be established, without prolonging the conventional MRI protocol duration. With the ^{2}H pulse acquisitions interleaved to all MRI sequences, more averages of ^{2}H signal can also be acquired, further improving the SNR of DMI.

Some MRI methods, like those employing short TRs, do not allow the direct insertion of a long DMI acquisition window. For those methods, the presented interleaving strategy may need to be adapted. Viable alternatives includes the use of gradient-echo-based DMI[30]. Alternatively, multiple short DMI acquisition windows can be used to acquire a truncated FID, which can be then fitted in the time domain.

The phase rolling of the up-converted ^{2}H signal stems from a lack of synchronization between the system LO and the external LO signal source. Previously, the frequency conversion approach has been described on clinical MRI scanners to acquire interleaved signals.[21] The phase rolling of the converted x-nucleus signal was also observed and was removed through postprocessing. Our device is able to remove the phase rolling in the interleaved signal in real time so that signal averaging and DMI reconstruction can be conveniently performed without additional postprocessing.

In theory, the phase rolling of upconverted signal can be calculated given the sequence timings, the frequency of the system receivers and that of the mixer. In reality, the presence of extensive looping structures, unknown (hidden) delays and eddy currents all lead to uncertainty in pulse sequence timing, making a robust and reliable phase prediction difficult to impossible. Fortunately, once MRI and DMI sequence timings are established, the phase accumulation is highly reproducible. Thus, a list approach in which the phases are measured and subsequently applied in parallel to the sequence, is able to compensate for these aberrations and allows phase locking for any sequence arrangement. The pre-generated phase list remained effective over the 30-day period we evaluated. A slightly increased phase fluctuation after 1 month suggests that there might be an overall drift effect over a long period of time and the phase stability performance in the long term can be further investigated.

The interleaved FLAIR and DMI scan offered a reasonable brain coverage, with freedom to adjust the MRI slice thickness and positions. In addition, the ^{1}H and ^{2}H pulses were selected such that they are able to accommodate the power requirements of most in-vivo scans (110 Hz – 140 Hz) using our ^{1}H-^{2}H head coil without changing pulse lengths. For these reasons, we were able to maintain the sequence time among all the in-vivo measurements, thus using a single phase list for the acquisitions. However, the use of a pre-acquired phase list and the general requirement for mutual timing of acquisitions do limit the impromptu adaptations of

scan parameters which are not uncommon in clinical scans (e.g. adaptations in number of slices, changes of TR, TE due to minimal pulse lengths adaptations or SAR restrictions in the consideration of available B_1^+). While this hurdle is best resolved with a vendor-supplied interleaved option, an alternative would be the use of a small, external reference signal combined with post-acquisition phase correction.

Interleaved MRI-DMI enriches the information content of an MRI study as the ^{2}H-based metabolic information is acquired in parallel with the ^{1}H-based anatomical image. The metabolic information provided by DMI can be supplemented by that provided by PET. Using the presented methodology, combined PET-MRI-DMI studies appears feasible on dedicated PET/MRI scanners. In addition to disease detections, correlating ^{2}H- and ^{1}H-based scans can provide novel opportunities to address various questions. For instance, interleaved fMRI-DMI can be used to study brain bioenergetics and acquire brain activation maps with near-identical timing. Furthermore, ^{1}H MRSI-DMI can be acquired to study the connections between biochemical composition and active metabolism in the tissue.

The interleaved MRI-DMI routine and hardware modifications we present here also provide a framework to develop other novel multi-nucleus acquisition methodologies. Other X-nuclei with similarly simple acquisition methods include ^{7}Li, ^{17}O, ^{23}Na and ^{31}P are equally suitable for interleaved MRI acquisitions and can follow the presented frequency-conversion strategy without significant modification.

Conclusions

Interleaved acquisition of MRI and an X-nucleus-based MR method is an excellent strategy to reduce scan time without sacrificing data quality. Interleaved MRI-DMI is attractive for clinical applications as it essentially doubles the information content of an MRI study by obtaining both anatomical data and information on active metabolism. In addition, the presented methodology is sufficiently flexible to accommodate most, if not all, MRI methods and provides a framework for other innovative multi-nucleus interleaved acquisitions.

Acknowledgements

The authors thank Monique Thomas for phantom preparations. Funding support comes from NIH grant NIBIB R01-EB025840.

References

1. Edelman RR, Hesselink JR, Zlatkin MB. Clinical magnetic resonance imaging. Saunders; 1996.
2. Buxton RB. Introduction to functional magnetic resonance imaging: principles and techniques. Cambridge university press; 2009.
3. Johansen-Berg H, Behrens TE. Diffusion MRI: from quantitative measurement to in vivo neuroanatomy. Academic Press; 2013.
4. Läsche M, Emons G, Gründker C. Shedding New Light on Cancer Metabolism: A Metabolic Tightrope Between Life and Death. Front Oncol. 2020;10:409–409. [PubMed: 32300553]
5. Pavlova NN, Thompson CB. The Emerging Hallmarks of Cancer Metabolism. Cell metabolism. 2016;23(1):27–47. [PubMed: 26771115]

6. Zilberter Y, Zilberter M. The vicious circle of hypometabolism in neurodegenerative diseases: Ways and mechanisms of metabolic correction. J Neurosci Res. 2017;95(11):2217–2235. [PubMed: 28463438]
7. Astrup J, Siesjö BK, Symon L. Thresholds in cerebral ischemia-the ischemic penumbra. Stroke. 1981;12(6):723–725. [PubMed: 6272455]
8. De Feyter HM, Behar KL, Corbin ZA, et al. Deuterium metabolic imaging (DMI) for MRI-based 3D mapping of metabolism in vivo. Science Advances. 2018;4(8):eaat7314. [PubMed: 30140744]
9. Lu M, Zhu X-H, Zhang Y, Mateescu G, Chen W. Quantitative assessment of brain glucose metabolic rates using in vivo deuterium magnetic resonance spectroscopy. Journal of Cerebral Blood Flow & Metabolism. 2017;37(11):3518–3530. [PubMed: 28503999]
10. Kreis F, Wright AJ, Hesse F, Fala M, Hu D-e, Brindle KM. Measuring Tumor Glycolytic Flux in Vivo by Using Fast Deuterium MRI. Radiology. 2019;294(2):289–296. [PubMed: 31821119]
11. Riis-Vestergaard MJ, Laustsen C, Mariager CØ, Schulte RF, Pedersen SB, Richelsen B. Glucose metabolism in brown adipose tissue determined by deuterium metabolic imaging in rats. International Journal of Obesity. 2020.
12. Wang T, Zhu X-H, Li H, et al. Noninvasive assessment of myocardial energy metabolism and dynamics using in vivo deuterium MRS imaging. Magnetic Resonance in Medicine. 2021;n/a(n/a).
13. Ruhm L, Avdievich N, Ziegs T, et al. Deuterium Metabolic Imaging in the human brain at 9.4 Tesla with high spatial and temporal resolution. Neuroimage. 2021:118639. [PubMed: 34637905]
14. Rich LJ, Bagga P, Wilson NE, et al. 1H magnetic resonance spectroscopy of 2H-to-1H exchange quantifies the dynamics of cellular metabolism in vivo. Nature Biomedical Engineering. 2020;4(3):335–342.
15. Chang LH, Shirane R, Weinstein PR, James TL. Cerebral metabolite dynamics during temporary complete ischemia in rats monitored by time-shared 1H and 31P NMR spectroscopy. Magn Reson Med. 1990;13(1):6–13. [PubMed: 2319935]
16. Chang LH, Cohen Y, Weinstein PR, Chileuitt L, James TL. Interleaved 1H and 31P spectroscopic imaging for studying regional brain injury. Magn Reson Imaging. 1991;9(2):223–227. [PubMed: 2034056]
17. Gonen O, Murphyboesch J, Srinivasan R, et al. Simultaneous and Interleaved Multinuclear Chemical-Shift Imaging, a Method for Concurrent, Localized Spectroscopy. Journal of Magnetic Resonance, Series B. 1994;104(1):26–33. [PubMed: 8025812]
18. Gonen O, Hu J, Murphy-Boesch J, Stoyanova R, Brown TR. Dual interleaved 1H and proton-decoupled-31P in vivo chemical shift imaging of human brain. Magn Reson Med. 1994;32(1):104–109. [PubMed: 8084223]
19. Friedman SD, Jensen JE, Frederick BB, Artru AA, Renshaw PF, Dager SR. Brain changes to hypocapnia using rapidly interleaved phosphorus-proton magnetic resonance spectroscopy at 4 T. J Cereb Blood Flow Metab. 2007;27(3):646–653. [PubMed: 16896347]
20. de Bruin PW, Koken P, Versluis MJ, et al. Time-efficient interleaved human (23)Na and (1)H data acquisition at 7 T. NMR Biomed. 2015;28(10):1228–1235. [PubMed: 26269329]
21. Meyerspeer M, Magill AW, Kuehne A, Gruetter R, Moser E, Schmid AI. Simultaneous and interleaved acquisition of NMR signals from different nuclei with a clinical MRI scanner. Magnetic Resonance in Medicine. 2016;76(5):1636–1641. [PubMed: 26608834]
22. Yu Z, Madelin G, Sodickson DK, Cloos MA. Simultaneous proton magnetic resonance fingerprinting and sodium MRI. Magnetic Resonance in Medicine. 2020;83(6):2232–2242. [PubMed: 31746048]
23. Niess F, Schmid AI, Bogner W, et al. Interleaved (31) P MRS/(1) H ASL for analysis of metabolic and functional heterogeneity along human lower leg muscles at 7T. Magn Reson Med. 2020;83(6):1909–1919. [PubMed: 31846116]
24. Kaggie JD, Sapkota N, Thapa B, et al. Synchronous radial 1H and 23Na dual-nuclear MRI on a clinical MRI system, equipped with a broadband transmit channel. Concepts in Magnetic Resonance Part B: Magnetic Resonance Engineering. 2016;46B(4):e21347.
25. Yale-School-of-Medicine. Deuterium Metabolic Imaging. https://medicine.yale.edu/lab/dmi/. Published 2019. Updated 01/15/2020. Accessed2021.

26. Hajnal JV, Bryant DJ, Kasuboski L, et al. Use of fluid attenuated inversion recovery (FLAIR) pulse sequences in MRI of the brain. J Comput Assist Tomogr. 1992;16(6):841–844. [PubMed: 1430427]

27. Hajnal JV, De Coene B, Lewis PD, et al. High signal regions in normal white matter shown by heavily T2-weighted CSF nulled IR sequences. J Comput Assist Tomogr. 1992;16(4):506–513. [PubMed: 1629405]

28. Lu H, Nagae-Poetscher LM, Golay X, Lin D, Pomper M, van Zijl PCM. Routine clinical brain MRI sequences for use at 3.0 Tesla. Journal of Magnetic Resonance Imaging. 2005;22(1):13–22. [PubMed: 15971174]

29. Mehan WA Jr., González RG, Buchbinder BR, et al. Optimal brain MRI protocol for new neurological complaint. PloS one. 2014;9(10):e110803–e110803. [PubMed: 25343371]

30. Peters DC, Markovic S, Bao Q, et al. Improving deuterium metabolic imaging (DMI) signal-to-noise ratio by spectroscopic multi-echo bSSFP: A pancreatic cancer investigation. Magnetic Resonance in Medicine. 2021;86(5):2604–2617. [PubMed: 34196041]

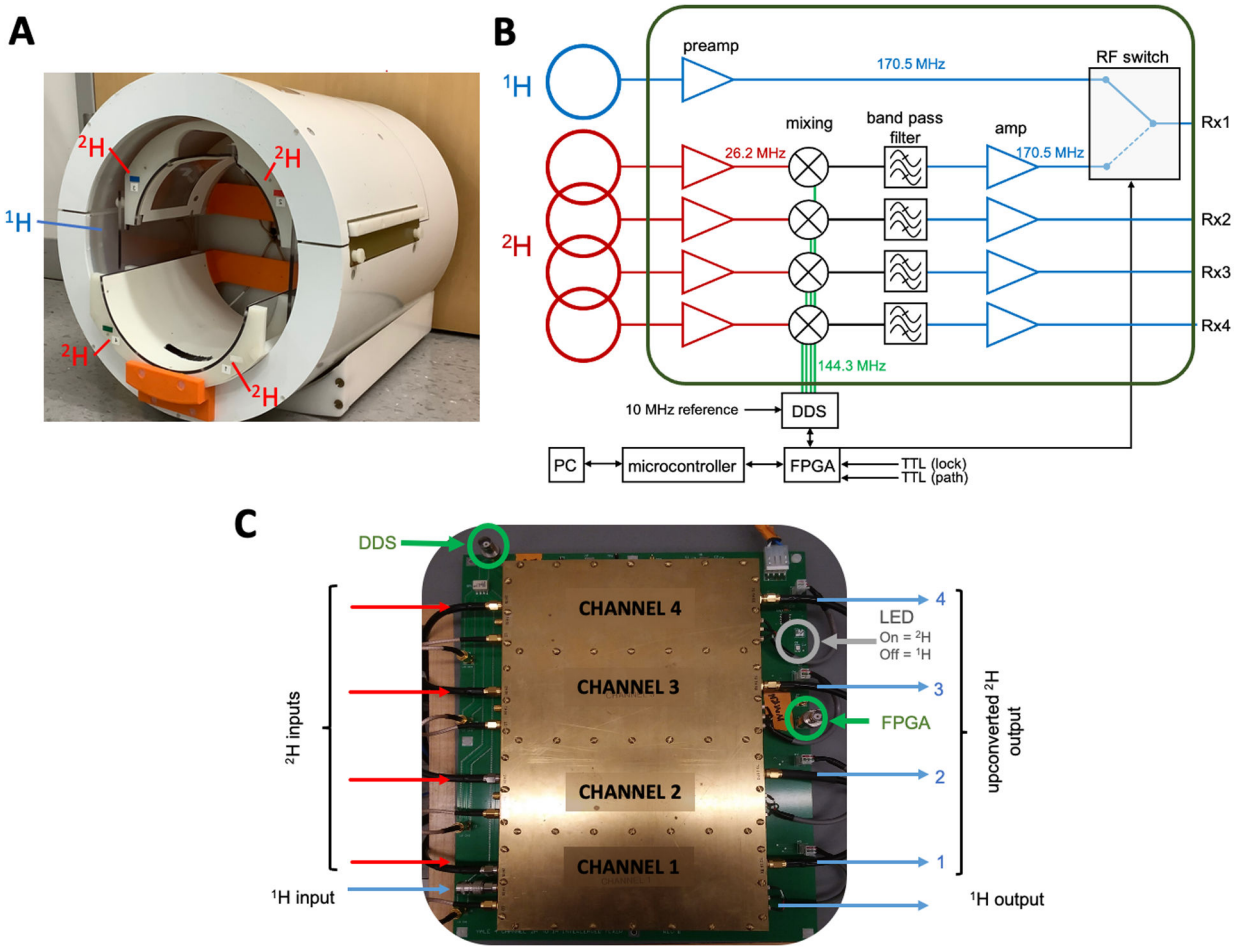

Figure 1.

Hardware used in interleaved 1H-2H imaging. **(A)** A photo of the 1H-2H coil used to conduct the measurements. The custom-built 1H-2H probe contains a transverse electromagnetic (TEM) volume coil (blue) tuned to 1H frequency and a four-coil phased array (red) tuned to 2H frequency. **(B)** Configuration of the frequency-conversion unit. The 1H signal is sent to one arm of an RF switch. The 2H signal at 26.2 MHz is supplied to an RF mixer and up-converted to 170.5 MHz by mixing with the 144.3 MHz Direct Digital Synthesizer (DDS) Local Oscillator (LO). This signal is band-pass-filtered, amplified and sent to the other arm of the RF switch. During MRI-DMI acquisitions, the RF switch, and the phase and frequency of DDS are controlled in real-time through a field-programmable gate array (FPGA) via TTL triggers and a network PC. **(C)** Photo of the integrated circuit that consists of the components in the green box in **(B)**. Note that the individual 2H channels are separated by brass walls in order to minimize channel-to-channel and external noise interference.

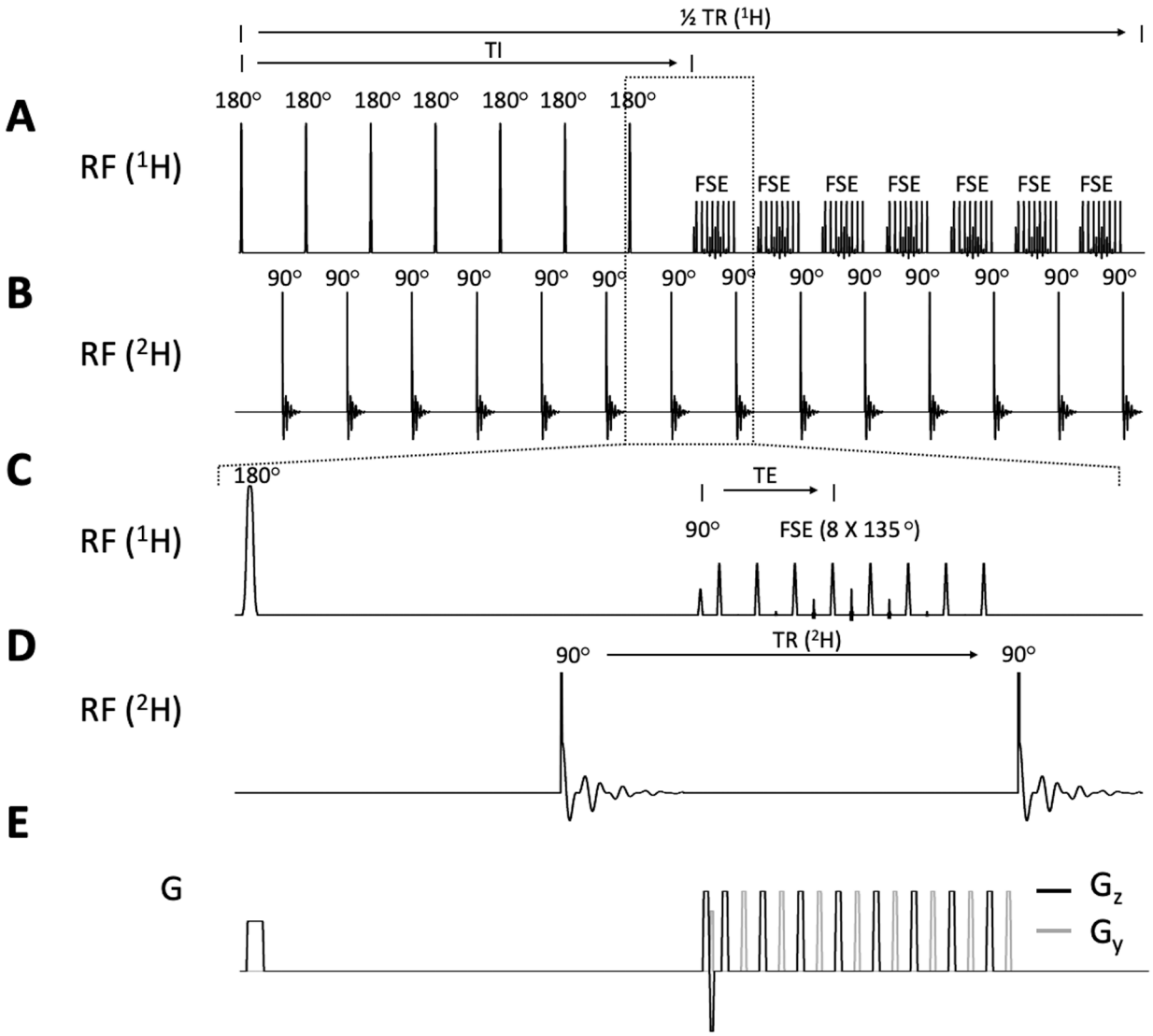

Figure 2.

Interleaved FLAIR-DMI sequence. **(A)** 1H pulse acquisition scheme depicting a multi-slice FLAIR MR method. 7 slices are inverted consecutively followed by a fast spin-echo (FSE) acquisition (TR/TI/TE = 8800/2200/90ms). The 2H pulse acquisitions **(B)** are placed in the dead time during TI and right after FSE with equal TR (= 314 ms). A selected part of the sequence (indicated by the dashed-line square) is zoomed in to show detailed 1H and 2H RF pulse-acquisition schemes **(C-D)** as well as the gradients arrangements **(E)**. Note that only the half of FLAIR MRI repetition time is illustrated (4400 ms). The second set of 7 slices is acquired during the second half for a total TR of 8800 ms. 28 DMI acquisitions are achieved in one FLAIR TR.

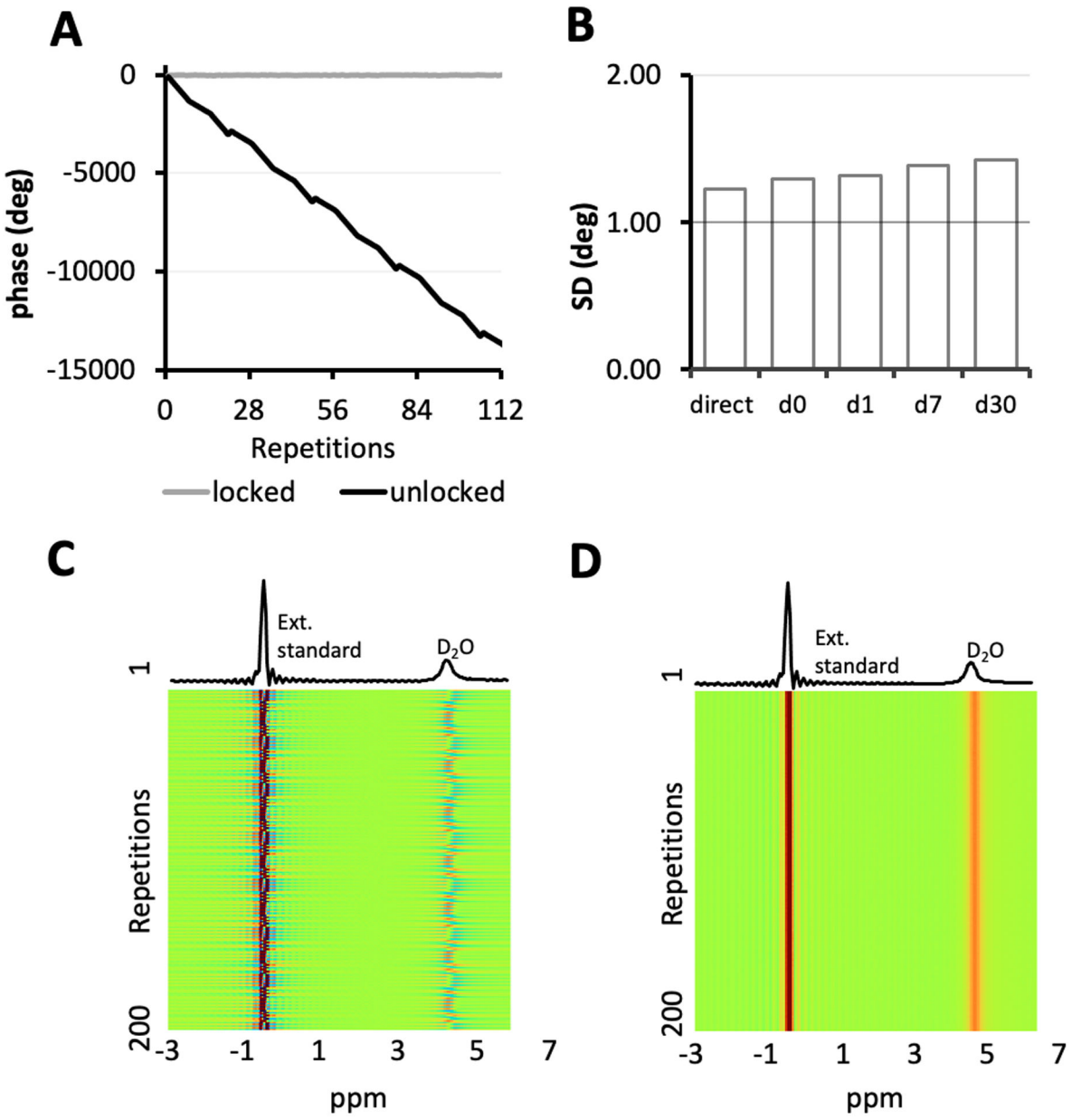

Figure 3.

Phase accumulation and phase locking of the upconverted 2H signal. **(A)** Phase accumulation (in degrees) is introduced to the upconverted 2H signal upon frequency mixing. By controlling the phase of DDS, phase-locking of the output signal can be achieved in real-time. **(B)** The standard deviation (SD) over the phase of the phase-locked 2H signal (i.e. gray curve in **(A)**) on the 0th, 1st, 7th and 30th day after the phase list was measured is compared with that of the direct 2H signal. Using the interleaved FLAIR-DMI sequence, global spectra of a D2O phantom and an external reference were collected without **(C)** and with **(D)** phase locking.

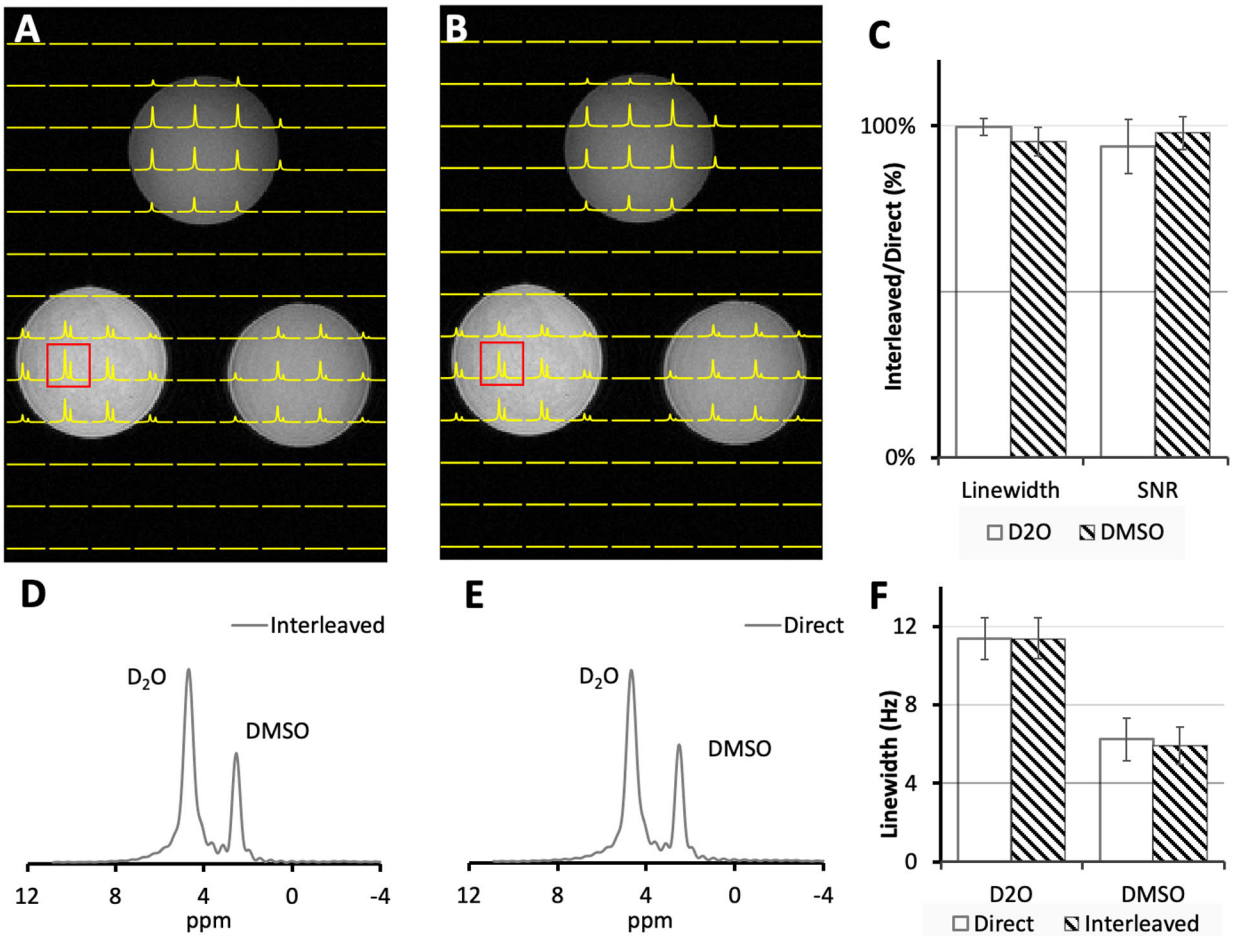

Figure 4.

(A) Interleaved DMI and FLAIR MRI and **(B)** Direct DMI of a phantom containing ~0.5% D2O and various amounts of DMSO-D6 (~0.02 – 0.05%) acquired as a 13 × 9 × 11 matrix over a 260 × 180 × 220 mm FOV using a spherical k-space encoding scheme. The spectra on the axial section displayed in **(A)** and **(B)** were apodized using 5 Hz exponential decay to reduce the truncation effect and fitted using LCM to obtain D2O and DMSO-D6 peak linewidth. The SNR were directly measured on the spectra. **(C)** The linewidth, SNR of direct and interleaved spectra were compared pixel to pixel. 2H spectra shown in **(D)** and **(E)** correspond to the highlighted red voxel in **(A)** and **(B)** respectively. The linewidth of 2H spectra in the displayed axial section were fitted and compared **(F)**. The error bars in the bar charts represent the standard deviation (SD) of the measurements.

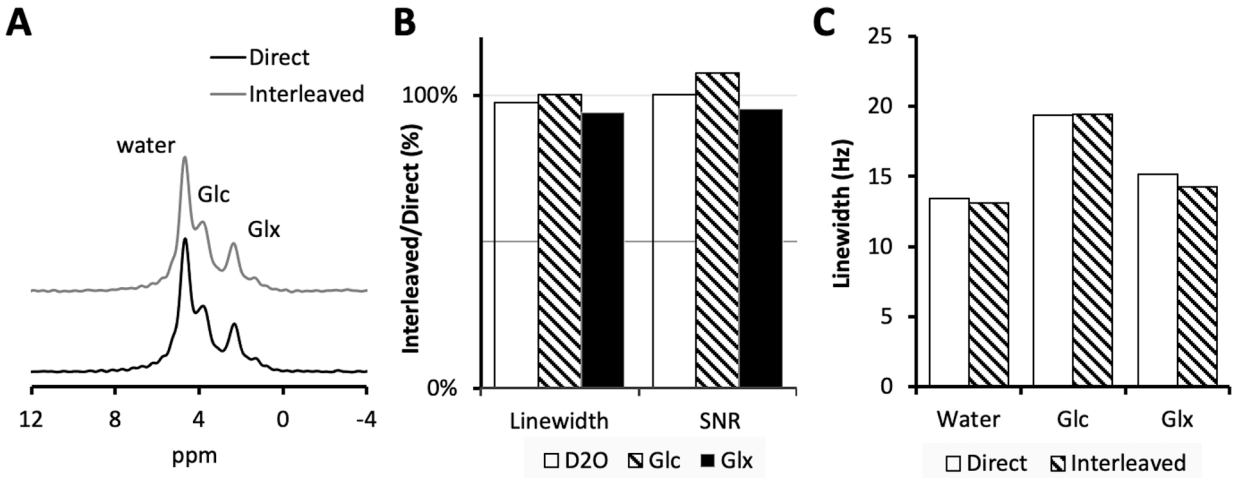

Figure 5.

(A) Direct and interleaved 2H global spectra acquired from human brain, 60 min following oral [6,6'−2H2]-glucose administration. The spectra were fitted using LCM fitting through least-squares minimization. **(B)** The fitted linewidth and SNR of the interleaved spectra relative to that of the direct spectra. **(C)** The fitted spectral linewidth of the direct and interleaved signal.

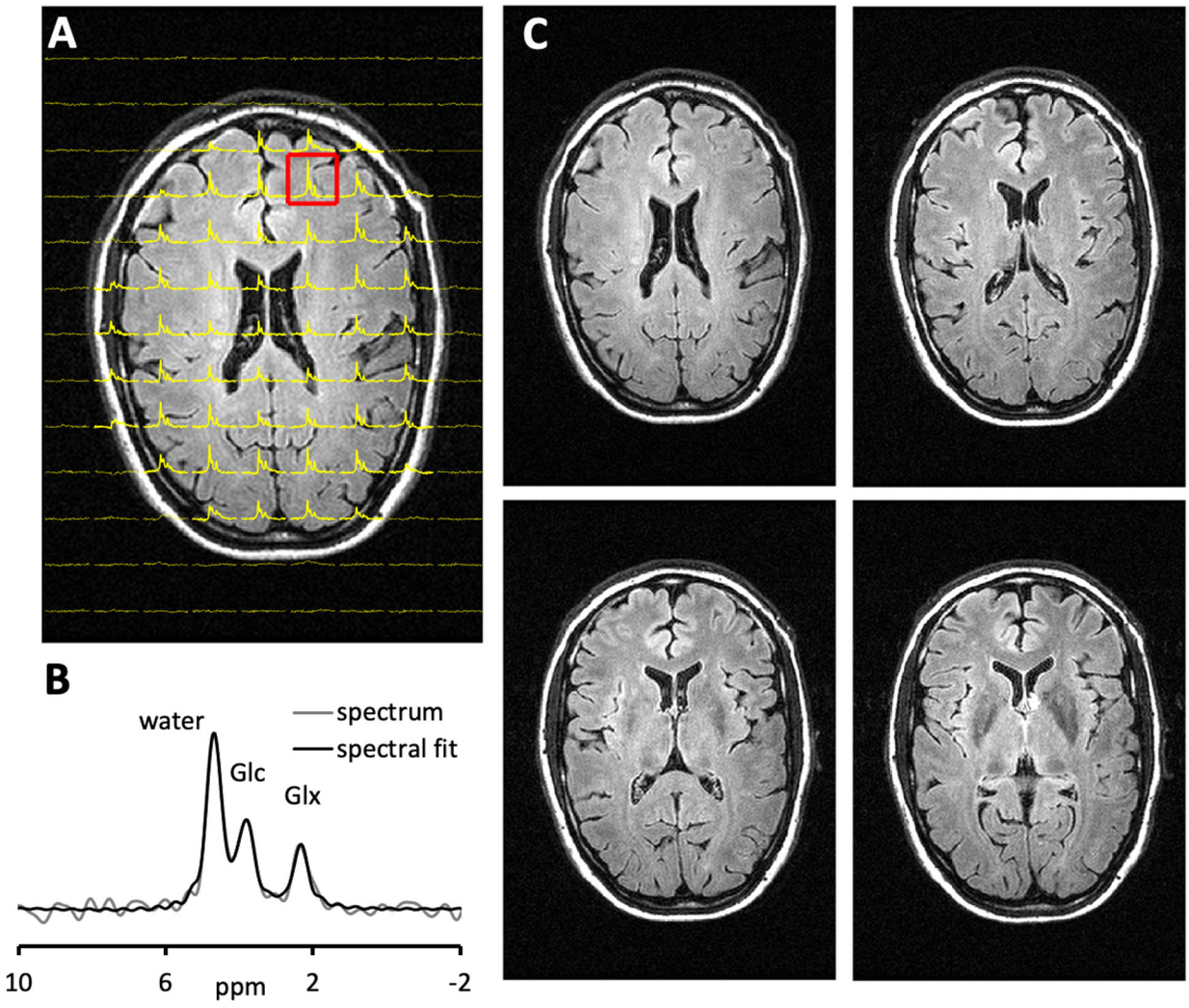

Figure 6.

Interleaved FLAIR and DMI of human brain 75 min following the oral administration of [6,6′-$^{2}H_2$]- glucose. (A) DMI was acquired as a 13 × 9 × 11 matrix over a 260 × 180 × 220 mm FOV(YXZ), whereas the FLAIR images were acquired as 14 slices and a 256 × 192 matrix over a 256 × 192 mm FOV (TR/TI/TE = 8800/2200/90 ms). During the ~7 min FLAIR acquisition, the DMI data could be acquired twice (i.e., NA = 2). (B) The magnified ^{2}H spectrum corresponding to the highlighted voxel in (A) is shown. (C) FLAIR images spanning circa 20 mm, covering the corresponding axial plane from the 3D DMI dataset as shown in (A)